# Neural Network-based Doppler Estimation for Orthogonal Time Frequency Space Systems

Peng Chen School EECMS Curtin University Bentley, WA, Australia peng.chen@curtin.edu.au Yue Rong
School EECMS
Curtin University
Bentley, WA, Australia
y.rong@curtin.edu.au

Abstract—Orthogonal time frequency space (OTFS) modulation has emerged as a promising technique for high-mobility communication scenarios due to its robustness against doublydispersive channels. Unlike the orthogonal frequency-division multiplexing (OFDM) technique, OTFS operates in the delay-Doppler (DD) domain, offering superior performance in environments with significant Doppler shifts. This paper proposes a deep neural network (DNN)-based Doppler estimation method integrated into an OTFS receiver. By leveraging fully-connected neural networks (FCNNs), the proposed system effectively learns to estimate Doppler shifts from received OTFS signals under various signal-to-noise ratio (SNR) conditions. Different input window sizes are examined to analyze network performance, revealing a trade-off between noise robustness and overfitting. Simulation results demonstrate that appropriately tuned FCNNs can provide accurate Doppler estimation, which significantly improves OTFS receiver performance in high-mobility settings.

## I. INTRODUCTION

The orthogonal frequency-division multiplexing (OFDM) technique is the key physical-layer modulation scheme adopted by 4G and 5G mobile systems. This technique is well-known for its robustness and high spectral efficiency in time-invariant frequency-selective channels, where the Doppler effect is limited and inter-symbol interference (ISI) is the primary factor limiting communication performance [1].

However, emerging mobile applications—such as low-earthorbit (LEO) satellites, autonomous vehicles, high-speed railways, and unmanned aerial vehicles (UAVs)—introduce new challenges due to their highly dynamic nature [2]. In such environments, wireless channels become doubly-dispersive, exhibiting both time dispersion due to multipath propagation and frequency dispersion caused by Doppler shifts [3]. These Doppler shifts result in inter-carrier interference (ICI) in OFDM systems, significantly degrading their performance [4].

To address this limitation, orthogonal time frequency space (OTFS) modulation was first proposed in [5], [6]. Compared to the OFDM system proposed in [7], which receives multiple linearly precoded OFDM symbols to provide time and frequency diversity, OTFS explicitly introduces a precoding technique that transforms the time-varying multipath channel into a 2D channel in the delay-Doppler (DD) domain, making it time-independent and constant. OTFS introduces an explicit precoding mechanism that maps information symbols into the delay-Doppler (DD) domain. This transformation renders

the channel representation quasi-static and independent of time variations. OTFS modulation distributes each information symbol across the entire time-frequency space via a set of 2D orthogonal basis functions—using inverse discrete Fourier transform (IDFT) along the Doppler axis and discrete Fourier transform (DFT) along the delay axis—thereby ensuring all transmitted symbols experience a nearly uniform channel gain in the DD domain [8]. This inherent property enhances the robustness of OTFS systems under severe Doppler effects.

The performance of OTFS systems has been evaluated in high-Doppler fading channels [9] and static multipath channels [10]. To demodulate interference-affected signals, various receiver designs have been proposed in the literature.

Channel estimation is a crucial element of OTFS demodulation. An impulse-based delay-Doppler domain channel estimation algorithm is described in [11] and further improved in [12]. This scheme transmits an impulse in the delay-Doppler domain as the training pilot. The received signals can be considered as a 2D periodic convolution of the transmitted impulse with the delay-Doppler channel in the delay-Doppler domain. Consequently, the delay-Doppler channel can be determined from the received signal using a threshold method. This scheme is extended to multiple-input multipleoutput (MIMO)-OTFS systems, where multiple impulses are transmitted with proper guards between adjacent impulses to distinguish channels from different antennas [13]. The method described may lead to inefficient usage of the time-frequency resource due to the guards while the actual Doppler shifts remain unknown.

In parallel, deep learning (DL) and deep neural network (DNN) have emerged as powerful tools for solving complex optimization and estimation problems in wireless communication systems [14]. For instance, a DNN model was developed in [15] to classify the type of traffic in received signals, while [16] proposed a DL-based channel estimation scheme for massive MIMO systems. Similarly, DNN-based estimators have been designed for underwater acoustic (UA) OFDM systems in [17], [18], demonstrating strong generalization capabilities and performance gains. In [19], a DNN was applied to a multi-objective resource allocation problem under multiple system constraints.

Motivated by these advances, this paper proposes an OTFS-

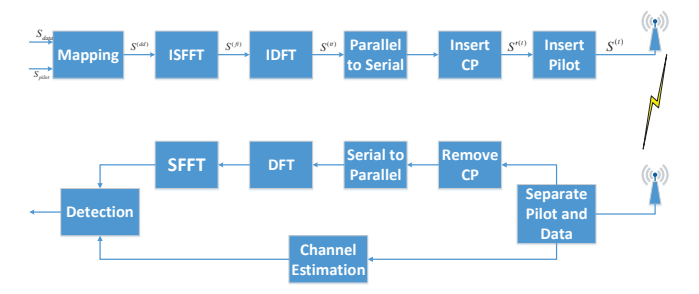


Fig. 1: Pilot-aided OTFS transceiver

based receiver that integrates a DNN-based Doppler estimator. The proposed system is designed to estimate the Doppler shifts of multipath components within a given delay period.

The contributions of this work lie in the development and evaluation of DNN-based receiver architectures for robust Doppler shift estimation in time-varying multipath channels. To facilitate model training and evaluation, large-scale datasets are generated across a wide range of signal-to-noise (SNR) levels, encompassing both single-path and two-path channel scenarios with identical delays. Extensive simulations using different window sizes are conducted to assess performance under various channel conditions, demonstrating the robustness of the proposed method to noise.

The remainder of this paper is organized as follows. Section II describes the system model, including the OTFS transceiver, channel assumptions, and the proposed Doppler shift estimation approach. Section III presents the DNN architectures, training procedure, hyperparameter settings, and implementation details of the proposed model. Section IV reports numerical simulation results and performance comparisons across various SNR levels. Finally, section V summarizes the important discoveries of this work.

# II. SYSTEM MODELS

# A. OTFS System

The proposed pilot-aided OTFS system is demonstrated in Fig. 1. The OTFS system transmits symbols across a 2D delay-Doppler (DD) domain lattice. It consists of  $N_{sc}$  subcarriers and  $N_{bl}$  blocks in the time-frequency (TF) domain, each OTFS symbol being prefixed with a cyclic prefix (CP) of  $N_{cp}$ samples. With sampling interval  $T_s$ , the subcarrier spacing is given by:

$$f_{\Delta} = \frac{1}{T_c N_{cc}}. (1)$$

The system bandwidth is  $B_o = N_{sc} f_{\Delta}$ , and the OTFS symbol duration is  $T_o = T_s N_{sc} N_{bl} + T_s N_{cp}$ .

## B. OTFS Modulation

A quadrature amplitude modulation (QAM)-modulated data sequence with a pilot symbol is arranged in the DD domain

$$\mathbf{\Lambda}^{(dd)} = \left\{ \frac{kf_{\Delta}}{N_{bl}}, \ lT_s \right\}, \quad 0 \le k < N_{bl}, \ 0 \le l < N_{sc} \quad (2)$$

This DD-domain matrix  $\mathbf{S}^{(dd)}$  is transformed into a timefrequency (TF) domain matrix  $S^{(tf)}$  inverse symplectic finite Fourier transform (ISFFT):

$$\mathbf{S}^{(tf)} = \mathbf{F}_{sc} \left( \mathbf{F}_{bl}^H \mathbf{S}^{(dd)} \right)^T \tag{3}$$

where  $\mathbf{F}_{sc}$  and  $\mathbf{F}_{bl}$  are DFT matrices of sizes  $N_{sc}$  and  $N_{bl}$ ,

Each TF block column is then transformed using an inverse DFT to obtain the time-domain blocks:

$$\mathbf{S}^{(tt)} = \mathbf{F}_{sc}^{H} \mathbf{S}^{(tf)} = \left(\mathbf{F}_{bl}^{H} \mathbf{S}^{(dd)}\right)^{T}.$$
 (4)

Serializing  $S^{(tt)}$  column-wise yields the 1D time-domain sequence  $\mathbf{s}^{\prime(t)}$ . CP is prepended to form the transmitted signal

$$s_n^{(t)} = \begin{cases} s_{N_{bl}N_{sc} - N_{cp} + n}^{\prime(t)} & 0 \le n < N_{cp} \\ s_{n - N_{cn}}^{\prime(t)} & N_{cp} \le n < N_{cp} + N_{sc}N_{bl} \end{cases}.$$

After pulse shaping with  $g_t(t)$ , the continuous-time transmitted signal is:

$$s(t) = \sum_{m=0}^{N_{bl}N_{sc} + N_{cp} - 1} s_m^{(t)} g_t(t - mT_s).$$
 (5)

#### C. Channel Model

We consider a doubly-dispersive, baseband time-varying channel with  $N_n$  paths, where each path has complex gain  $\alpha_n$ , delay  $\tau_n$ , and Doppler  $\nu_n$ . The DD-domain channel spreading function is given by

$$h_t(\tau, \nu) = \sum_{n=0}^{N_p - 1} \alpha_n \delta(\tau - \tau_n) \delta(\nu - \nu_n)$$
 (6)

where  $\delta(\cdot)$  denotes the Dirac delta function. The received signal is modeled as:

$$r(t) = \sum_{n=0}^{N_p - 1} \alpha_n e^{j2\pi\nu_n t} s(t - \tau_n) + w(t)$$
 (7)

where w(t) is analog additive white Gaussian noise (AWGN).

## D. OTFS Demodulation

At the receiver, the signal r(t) is matched-filtered with a predefined filter  $q_r(t)$  and sampled at intervals of  $T_s$ . After the CP is removed, the time-domain samples of an OTFS symbol are reshaped into a 2D block. DFT is applied along columns to obtain the TF domain signal, followed by the symplectic FFT (SFFT) to recover the DD-domain symbols.

Assuming that the resolution  $T_s$  is sufficient to approximate the path delays to the nearest sampling point in a typical wideband system, let  $\tau'_n$  denote the closest integer to  $\frac{\tau_n}{T_s}$ , for n= $\mathbf{\Lambda}^{(dd)} = \left\{ \frac{kf_{\Delta}}{N_{bl}}, \ lT_s \right\}, \quad 0 \leq k < N_{bl}, \ 0 \leq l < N_{sc} \quad \text{(2)} \quad \begin{array}{c} 0, 1, \cdots, N_p - 1. \text{ Then, the received signal } r_{k,l} \text{ at DD-domain} \\ \text{grid point } \mathbf{\Lambda}^{(dd)} = \left( \frac{kf_{\Delta}}{N_{bl}}, \ lT_s \right) \text{ is given by [11]:} \end{array}$ 

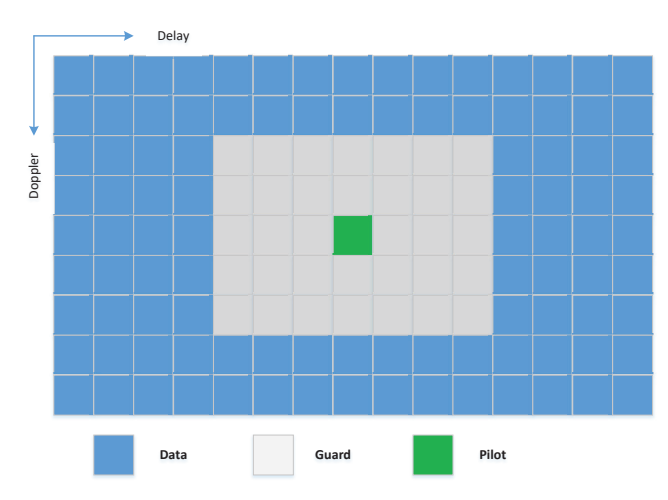


Fig. 2: Pilot-aided OTFS structure

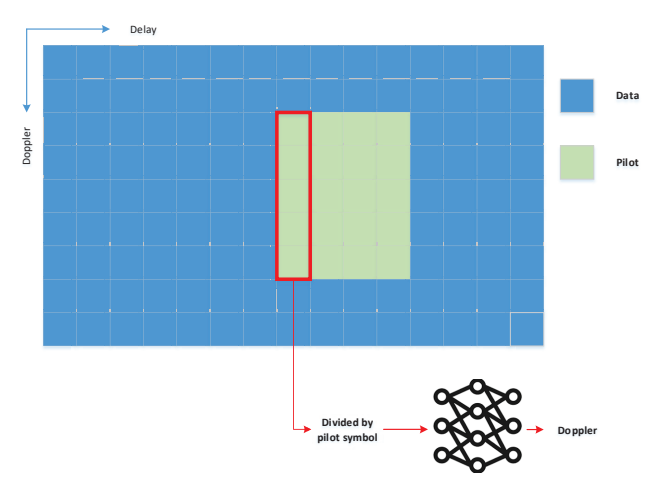


Fig. 3: Received pilot-aided OTFS symbol and Doppler estimation

$$r_{k,l} = \sum_{n=0}^{N_p - 1} \left\{ \sum_{q = -N_{bl}/2}^{N_{bl}/2 - 1} \left( \bar{\alpha}(q, \nu_n) \, \alpha_n \, \mathbf{S}_{[k+q]_{N_{bl}}, [l-\tau'_n]_{N_{sc}}}^{(dd)} \right. \right.$$

$$\times e^{-j2\pi\nu_n \tau'_n T_s} \right\} + v_{k,l}$$
(8)

where  $v_{k,l}$  is the AWGN noise at DD domain,  $[\cdot]_M$  denotes modulo M operation, and  $\bar{\alpha}(q,\nu_n)$  represents the fractional Doppler factor and is defined as:

$$\bar{\alpha}(q,\nu_n) = \frac{e^{j2\pi(-q-N_{sc}N_{bl}T_s\nu_n)} - 1}{N_{bl}e^{j\frac{2\pi}{N_{bl}}(-q-N_{sc}N_{bl}T_s\nu_n)} - N_{bl}}.$$
 (9)

The magnitude of (9) resembles a sampled Dirichlet sinc function shifted by  $N_{sc}N_{bl}T_s\nu_n$ , characterizing the amplitude distribution of fractional Doppler spreading in the Doppler axis.

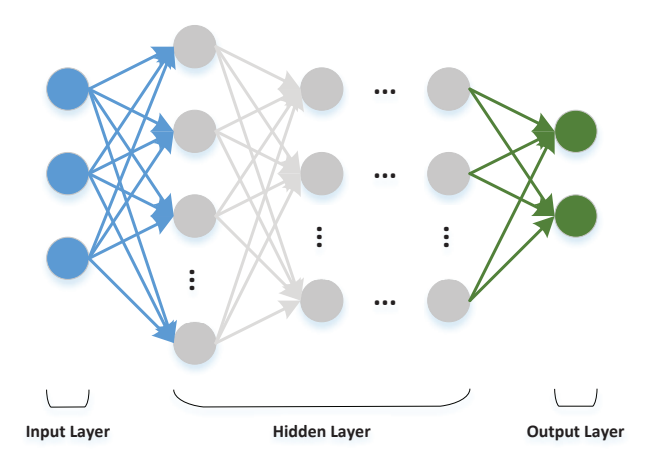


Fig. 4: Typical DNN structure.

# E. DNN-based Doppler Estimation

In this section, we consider a pilot-aided OTFS system as illustrated in Fig. 2 [11]. For each OTFS symbol, a single pilot symbol is inserted in the DD domain, with sufficient guard gaps along both the delay and Doppler axes. This ensures that the pilot region and the data region do not interfere with each other at the receiver, as shown in Fig. 3, allowing them to be separated. The region containing the pilot symbol is utilized for Doppler estimation.

We assume a very high sampling rate in the system, so that each column in the pilot region in DD domain corresponds to different and limited propagation paths, enabling independent channel estimation. A DNN is employed to estimate the Doppler shifts of these channel paths. The network input is a column from the pilot region, normalized by the transmitted pilot symbol to eliminate its influence.

# III. THE PROPOSED DNN-BASED DOPPLER ESTIMATOR

#### A. Deep Neural Network

Deep neural network is a subset of machine learning that has gained prominence due to its ability to automatically extract and process features from raw data without manual intervention. Inspired by the human brain, DNNs consist of multiple layers of interconnected neurons and are widely used in tasks such as classification, signal detection, and channel estimation.

While a single-layer network can approximate any function, deeper networks are more effective at capturing complex patterns. As shown in Fig. 4, a typical DNN includes an input layer, multiple hidden layers, and an output layer. The architecture—including the number of layers and neurons—is usually determined through experimentation. Activation functions are key to enabling nonlinear transformations and allow DNNs to approximate virtually any nonlinear function.

A common form of DNN is the fully connected neural network (FCNN), where each neuron in one layer connects to every neuron in the next layer. The fundamental unit of an FCNN is the perceptron, which computes a weighted sum of inputs plus a bias, followed by a nonlinear activation function. Training process is adopted to optimize these weights using backpropagation to minimize a predefined loss function.

The deployment of a DNN model typically involves two distinct phases: the training phase and the inference (working) phase. Prior to being applied for real-time applications, the DNN must undergo a comprehensive training process. The training process consists of two main steps: forward propagation, where input data is passed through the network layers to produce an output, and backpropagation, where the error between the predicted and actual outputs is propagated backward through the network to update weights and biases according to gradient descent rules. This iterative process continues until a stopping criterion is met, such as convergence of the loss function or reaching a predefined number of epochs.

In general, effective training is critical to the success of any DNN-based system. A sufficiently large and diverse dataset is required to ensure the network captures the full range of relevant feature. As discussed in Section II, a DNN model is employed to estimate Doppler shifts using a column of the received pilot signal. Given the constraints of limited computational and time resources during inference, a relatively simple yet efficient DNN architecture is adopted.

## B. The Proposed DNN Model

A DNN model is proposed for regression-based Doppler estimation, featuring a six-layer architecture comprising an input layer, four hidden layers, and an output layer. The proposed model consists of 257, 771, 514, 128, 64, and 2 neurons in successive layers according to the simulation settings in Section IV. The rectified linear unit (ReLU) activation function is employed in all layers except the output layer, for which the hyperbolic tangent (Tanh) function is adopted to produce bounded output values.

It is assumed that the SNR is known at the receiver, and the network input comprises both the received pilot signals and the corresponding SNR. Specifically, a window of length  $N_w$  centered at the transmitting pilot position is applied to the received pilot to retain the dominant Doppler components. The real and imaginary parts of this windowed pilot are separated and concatenated with the SNR value, forming a composite input feature vector. The corresponding labels are the Doppler shifts of two paths, normalized to the range [-1,1] using the maximum Doppler frequency.

To train and evaluate the proposed model, two independent datasets were generated: one for training and one for testing. The training dataset consists of two subsets—one with single-path channels and the other with two-path channels. Each subset contains samples across multiple SNR levels: 6,10,14,18,22,26,30,34 dB, with 10,000 samples per SNR level, resulting in a total of 160,000 training samples. The testing dataset spans SNR levels 6,8,10,12,14,16,18,20,22,24,26,28,30,32,34 dB, with 10,000 samples generated for each level.

When training the networks, the training dataset is partitioned into training and validation sets in an 8:2 ratio. The

network is trained using the mean-squared error (MSE) loss function (10), which is a standard choice for regression tasks.

$$e_{mse} = E\left[\frac{1}{2}\sum_{p=0}^{1}(\check{\nu}_{p} - \tilde{\nu}_{p})^{2}\right]$$
 (10)

where  $\nu_p$  denotes the normalized Doppler shift of the pth path and  $\nu_p$  denotes the corresponding estimated value. Optimization is performed using the Adam algorithm with a learning rate of 0.0001, facilitating efficient convergence of the model parameters.

#### IV. NUMERICAL RESULTS

In this section, we verify the proposed Doppler estimation algorithm through simulations. An OTFS symbol structure is considered with  $N_{sc}=512$  subcarriers and  $N_{bl}=128$  blocks, resulting in a DD-domain grid of size  $128\times512$ . The CP length is set to 20 samples. The subcarrier spacing is set to  $f_{\Delta}=15$  kHz, and the carrier frequency is configured at  $f_c=4$  GHz. The user equipment (UE) speed is assumed to be 120 km/h, which corresponds to a high-mobility scenario typical of vehicular or high-speed rail environments. Given this configuration, the Doppler resolution in the DD domain is 117.19 Hz, and the maximum Doppler shift is  $\nu_M=444.44$  Hz.

We consider a one-path or two-path channel model, where both paths share the same delay value set to 0. This configuration is representative of wideband wireless communication environments. For instance, under the above system settings, the 3GPP LTE Extended Vehicular A (EVA) channel model [20] typically contains no more than two multipath components within one sampling interval, making the above two-path assumption both practical and realistic for such scenarios. The Doppler shifts for each channel realization are generated based on Jakes' model, using the expression  $\nu = \nu_M \cos \theta$ , where  $\theta$  is a random variable uniformly distributed in the interval  $[-\pi,\pi]$ . Each path is modeled as a complex-valued random variable whose real and imaginary parts are independent Gaussian variables with zero mean and equal variance, resulting in a magnitude that follows a Rayleigh distribution. The variance of the real and imaginary components is 1/2 and 1/4 for onepath and two-path channels, respectively.

An example of DD-domain channel response of the received signal without noise is shown in Fig. 5. In this example, the channel contains two paths with delay 0 and different Doppler shifts. The amplitudes of the two paths are 0.568 and 0.624, respectively. The theoretical channel responses of the two paths are shown together with the amplitude of the received channel response. It can be observed that the left part follows the first path response while the right part follows the second path response. The maximum amplitude of the received response fails to reach the theoretical one. The result implies that the Doppler of the two paths can be estimated in this example as the amplitude of the first path response is sufficiently small when the second path response reaches maximum, and the amplitude of the second path response

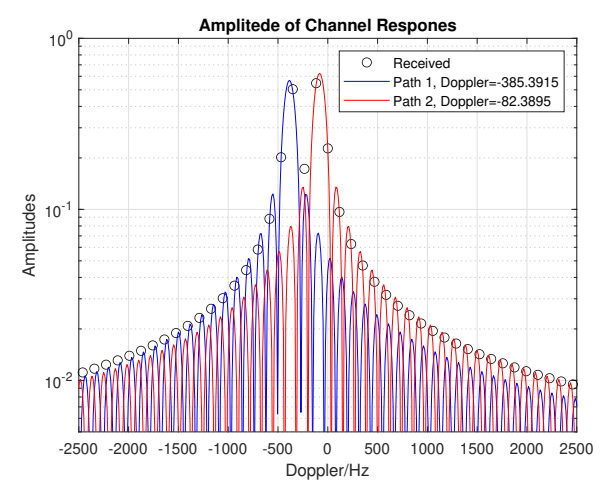


Fig. 5: DD-domain channel response of the received signal.

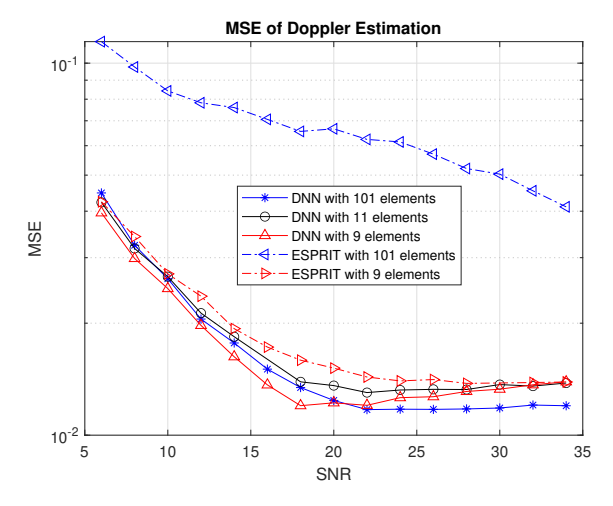


Fig. 6: MSE of Doppler estimation.

is sufficiently small when the first path response reaches maximum. It also implies that it is not necessary to take all the 128 elements within one column of the pilot region for Doppler estimation, as several middle elements already occupy dominant energy.

The performance of the trained networks using different window sizes (9, 11, and 101) is illustrated in Fig. 6 compared with the traditional estimation of signal parameters via rotational invariance techniques (ESPRIT) algorithm. The MSE between the estimated and true Doppler shifts (10) is used to evaluate the network performance.

The ESPRIT algorithm achieves performance comparable to the proposed DNN-based estimator with a window size of 9. Specifically, ESPRIT performs worse than the DNN at low SNRs but converges to a similar accuracy when the SNR exceeds 30 dB. In contrast, ESPRIT with a larger window size of 101 exhibits degraded performance due to its high sensitivity to the additional noise introduced by the extended window.

The network with a window size of 9 achieves the best performance for SNR values up to 20 dB. However, as the SNR exceeds 18 dB, its performance begins to degrade, suggesting an overfitting issue at higher SNRs. A similar trend is observed for the window size 11, though the degradation is smoother.

In contrast, the network trained with a window size of 101 exhibits poor performance at low SNRs (below 8 dB), due to the introduction of significant noise. However, its performance improves steadily with increasing SNR and outperforms the other two networks for SNR values above 22 dB. Importantly, no overfitting issue is observed in this network, as the larger window size likely contributes to better generalization in high-SNR conditions.

## V. CONCLUSION

This work presents a novel OTFS receiver architecture enhanced by a fully-connected deep neural network for Doppler shift estimation. The proposed method uses an embedded pilot and transforms received DD-domain pilot into Doppler estimates using a trained DNN, providing resilience against high-mobility impairments. Evaluations across different SNR levels and input window sizes show that smaller windows perform better at low SNRs but are prone to overfitting at high SNRs, while larger windows offer improved generalization in high SNR conditions. The results confirm that DNNs can serve as effective tools in channel parameter estimation, complementing traditional signal processing methods and enhancing the robustness of OTFS systems in dynamic wireless environments.

# REFERENCES

- H. Sampath, S. Talwar, J. Tellado, V. Erceg, and A. Paulraj, "A fourth-generation MIMO-OFDM broadband wireless system: design, performance, and field trial results," *IEEE Communications Magazine*, vol. 40, pp. 143–149, Sept. 2002.
- [2] Z. Wei, W. Yuan, S. Li, J. Yuan, G. Bharatula, R. Hadani, and L. Hanzo, "Orthogonal time-frequency space modulation: a promising next-generation waveform," *IEEE Wireless Communications*, vol. 28, pp. 136–144, Aug. 2021.
- [3] D. Tse and P. Viswanath, Fundamentals of Wireless Communication. USA: Cambridge University Press, 2005.
- [4] T. Wang, J. Proakis, E. Masry, and J. Zeidler, "Performance degradation of OFDM systems due to Doppler spreading," *IEEE Transactions on Wireless Communications*, vol. 5, pp. 1422–1432, June 2006.
- [5] R. Hadani, S. Rakib, A. F. Molisch, C. Ibars, A. Monk, M. Tsatsanis, J. Delfeld, A. Goldsmith, and R. Calderbank, "Orthogonal time frequency space (OTFS) modulation for millimeter-wave communications systems," in 2017 IEEE MTT-S International Microwave Symposium (IMS), pp. 681–683, June 2017.
- [6] R. Hadani, S. Rakib, M. Tsatsanis, A. Monk, A. J. Goldsmith, A. F. Molisch, and R. Calderbank, "Orthogonal time frequency space modulation," in 2017 IEEE Wireless Communications and Networking Conference (WCNC), pp. 1–6, Mar. 2017.
- [7] J. Han, S. P. Chepuri, Q. Zhang, and G. Leus, "Iterative per-vector equalization for orthogonal signal-division multiplexing over time-varying underwater acoustic channels," *IEEE Journal of Oceanic Engineering*, vol. 44, pp. 240–255, Jan. 2019.
- [8] T. Zemen, M. Hofer, D. Löschenbrand, and C. Pacher, "Iterative detection for orthogonal precoding in doubly selective channels," in 2018 IEEE 29th Annual International Symposium on Personal, Indoor and Mobile Radio Communications (PIMRC), pp. 1–7, Sept. 2018.
- [9] K. R. Murali and A. Chockalingam, "On OTFS modulation for high-Doppler fading channels," in 2018 Information Theory and Applications Workshop (ITA), pp. 1–10, Feb. 2018.

- [10] P. Raviteja, K. T. Phan, Y. Hong, and E. Viterbo, "Interference cancellation and iterative detection for orthogonal time frequency space modulation," *IEEE Transactions on Wireless Communications*, vol. 17, pp. 6501–6515, Oct. 2018.
- [11] P. Raviteja, K. T. Phan, and Y. Hong, "Embedded pilot-aided channel estimation for OTFS in delay–Doppler channels," *IEEE Transactions on Vehicular Technology*, vol. 68, pp. 4906–4917, May 2019.
- [12] Z. Wei, W. Yuan, S. Li, J. Yuan, and D. W. K. Ng, "Off-grid channel estimation with sparse Bayesian learning for OTFS systems," *IEEE Transactions on Wireless Communications*, vol. 21, pp. 7407–7426, Sept. 2022.
- [13] M. Kollengode Ramachandran and A. Chockalingam, "MIMO-OTFS in high-Doppler fading channels: signal detection and channel estimation," in 2018 IEEE Global Communications Conference (GLOBECOM), pp. 206–212, Dec. 2018.
- [14] J. Gao, C. Zhong, G. Y. Li, and Z. Zhang, "Online deep neural network for optimization in wireless communications," *IEEE Wireless Communications Letters*, vol. 11, pp. 933–937, May 2022.
- [15] T. J. O'Shea, S. Hitefield, and J. Corgan, "End-to-end radio traffic sequence recognition with recurrent neural networks," in 2016 IEEE Global Conference on Signal and Information Processing (GlobalSIP), pp. 277–281, Dec. 2016.
- [16] J. Gao, M. Hu, C. Zhong, G. Y. Li, and Z. Zhang, "An attention-aided deep learning framework for massive MIMO channel estimation," *IEEE Transactions on Wireless Communications*, vol. 21, pp. 1823–1835, Mar. 2022.
- [17] R. Jiang, X. Wang, S. Cao, J. Zhao, and X. Li, "Deep neural networks for channel estimation in underwater acoustic OFDM systems," *IEEE Access*, vol. 7, pp. 23579–23594, 2019.
- [18] S. Thenginthody Hassan, P. Chen, Y. Rong, and K. Y. Chan, "Underwater acoustic orthogonal frequency-division multiplexing communication using deep neural network-based receiver: river trial results," *Sensors*, vol. 24, p. 5995, Jan. 2024.
- [19] W. Lee, O. Jo, and M. Kim, "Intelligent resource allocation in wireless communications systems," *IEEE Communications Magazine*, vol. 58, pp. 100–105, Jan. 2020.
- [20] 3GPP, "Technical Specification Group Radio Access Network; Evolved Universal Terrestrial Radio Access (E-UTRA); Base Station (BS) radio transmission and reception," Technical Specification (TS) 36.104, 3rd Generation Partnership Project (3GPP), 04 2024. Version 18.5.0.